Structures of two RNA domains essential for hepatitis C virus internal ribosome entry site function

Peter J. Lukavsky[1], Geoff A. Otto[1], Alissa M. Lancaster[2], Peter Sarnow[2] and Joseph D. Puglisi[1]

[1]Department of Structural Biology and [2]Department of Microbiology and Immunology, Stanford University School of Medicine, Stanford, California 94305-5126, USA.

Translation of the hepatitis C virus (HCV) polyprotein is initiated at an internal ribosome entry site (IRES) element in the 5′ untranslated region of HCV RNA. The HCV IRES element interacts directly with the 40S subunit, and biochemical experiments have implicated RNA elements near the AUG start codon as required for IRES–40S subunit complex formation. The data we present here show that two RNA stem loops, domains IIId and IIIe, are involved in IRES–40S subunit interaction. The structures of the two RNA domains were solved by NMR spectroscopy and reveal structural features that may explain their role in IRES function.

Initiation of translation of the hepatitis C virus genome is mediated by an internal ribosome entry site (IRES) element in the 5′ untranslated region (5′ UTR) of HCV genomic RNA[1,2]. Normal translation initiation in eukaryotes occurs by recognition of the 5′ cap structure of the mRNA by eukaryotic initiation factor 4E (eIF4E) followed by assembly of other initiation factors and the 40S ribosomal subunit, and subsequent scanning of the 5′ UTR to the first AUG initiation codon[3]. In HCV, IRES-mediated initiation eliminates the requirement for the 5′ cap structure and scanning. The 40S subunit is recruited directly to the vicinity of the start codon by interaction with the IRES element; only a subset of the total translation initiation factors is required for this process[2]. As such, IRES-mediated initiation in HCV and related pestiviruses is reminiscent of prokaryotic translational initiation, in which the Shine-Dalgarno interaction between messenger RNA and 16S ribosomal RNA recruits 30S subunits directly to the start codon, and only three initiation factors are required[4]. How the IRES directly interacts with the 40S ribosomal subunit remains unclear.

The HCV IRES element is a complex RNA secondary structure consisting of nucleotides 44–354 in the 5′ UTR[5–8]. Biochemical experiments have demonstrated the roles of particular subdomains to IRES function. In particular, mutagenesis and functional data support a pseudoknot structure near the AUG start codon[9,10]. The sites of interaction with the 40S subunit have been mapped by toe-printing, which yielded strong, 40S-dependent primer extension stops in the IRES subdomains including and adjacent to the pseudoknot structure[4]. Mutations within two hairpin loops, domain IIId and IIIe, disrupt IRES-mediated initiation[11,12]. Biochemical and small angle X-ray scattering experiments suggested that the IRES has a metal-dependent tertiary structure, which may be required for interaction with 40S subunits[12].

We present here biochemical and functional data that support the direct role of domain IIId and IIIe hairpins in IRES interaction with the 40S subunit and we have determined the structures of these two RNA domains by NMR spectroscopy. Our results further support the role of IRES RNA structure in recognition of the 40S ribosomal subunit.

HCV IRES chemical footprinting

The HCV IRES binds directly to the 40S ribosomal subunit in the absence of external factors[4]. To map the regions of the IRES that may interact with 40S subunits, we performed chemical probing on the IRES RNA (domain IV and the 3′ half of domain III) in the absence or presence of ribosomal subunits. The chemical reactivity of the unbound IRES is consistent with the well-characterized secondary structure of the IRES (Fig. 1*a*). The reactivity of the bases depends on the Mg^{2+} concentration, consistent with the previously defined Mg^{2+}-dependent formation of tertiary structure for the IRES[12]. Upon binding of the folded IRES to 40S subunits, two regions of the IRES show strong changes in reactivity (Fig. 1*b*). The Watson-Crick faces of guanosines in the hairpin loops of domains IIId and IIIe are strongly reactive to kethoxal in the unbound IRES, and are almost completely protected upon 40S binding. In contrast, three adenosines in the stem of domain IIId show increases in reactivity upon 40S subunit binding. These loops are required for IRES function *in vivo* and *in vitro*[11,12] and our chemical probing experiments suggest that they are involved in IRES–40S subunit interaction.

NMR spectroscopy

To understand further the role of domains IIId and IIIe in IRES function, we determined both structures using NMR spectroscopy (Fig. 1*c*). For domain IIIe, a 14-residue RNA oligonucleotide, corresponding to nucleotides 291–302 was studied using homonuclear NMR methods. The spectra were readily assigned without isotopic labeling, and a total of 271 NOE and 88 dihedral torsion angle restraints were obtained. For domain IIId, a 29-residue RNA oligonucleotide, corresponding to nucleotides 253–279, was studied by NMR spectroscopy. A combination of homonuclear and heteronuclear 2D and 3D NMR methods yielded a total number of 705 NOE and 200 dihedral torsion angle restraints. Measurement of intra base pair $^2J_{NN}$ couplings across hydrogen bonds was employed to establish base pairing schemes[13]. For both hairpin loops, only NMR-derived restraints were used for structure calculations.

Structure of HCV IRES domain IIIe

The domain IIIe hairpin loop adopts a novel tetraloop fold and is well defined by the NMR data (heavy atom root mean square (r.m.s.) deviation = 0.89 Å; Fig. 2*a*). The helical stem of domain IIIe is terminated by a U294-G299 wobble pair, followed by a loop closing, sheared G295-A298 base pair (Fig. 2*b*). Similar pairing interactions are observed in the GNRA tetraloops and in purine-rich hexaloops[14,15]. The loop sequence (–GAUA–), however, does not conform to the standard GNRA motif and adopts a different structure. The bases of A296 and U297 point towards the major groove and are not involved in RNA backbone contacts that would stabilize the loop fold; the two central nucleotides of the tetraloop stack on the 5′ guanosine of the sheared G-A pair. This fold creates an array of three major groove exposed Watson-Crick faces (G295, A296, and U297). In contrast, the central purine and adenosine in a GNRA tetraloop point towards the minor

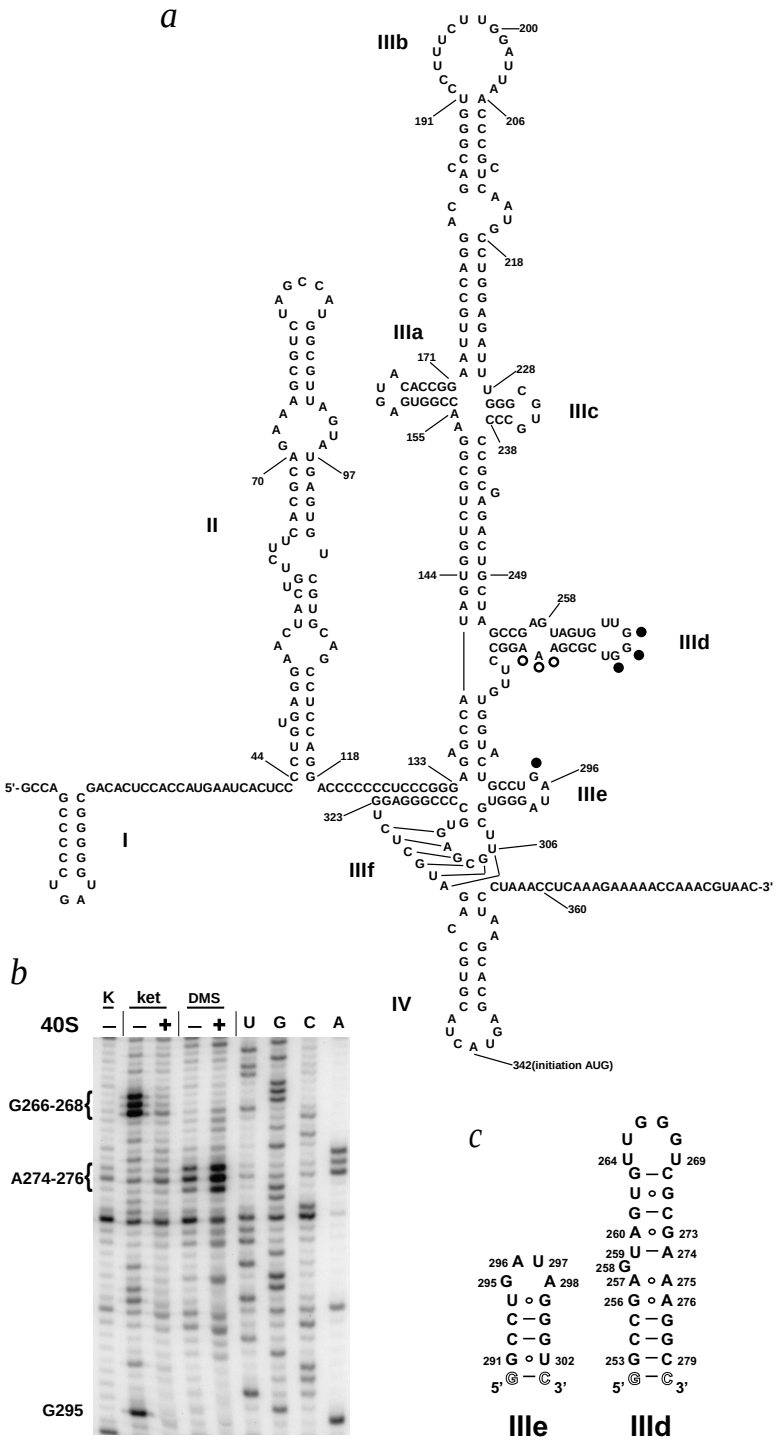

Fig. 1 ***a***, Sequence and secondary structure of HCV IRES RNA (nucleotides 1–383 of HCV genotype 1b). Domains are numbered according to ref. 34 Nucleotides protected from kethoxal modification upon 40S subunit binding are indicated by filled circles. Nucleotides that show increases in DMS modification upon 40S subunit binding are indicated by open circles. ***b***, Autoradiograph of kethoxal and DMS probing of HCV IRES RNA domains IIId and IIIe in the absence (–), or presence (+) of 40S subunits. The K lane is a primer extension reaction using the unmodified HCV IRES RNA. The kethoxal (ket) and DMS probing and primer extension reactions are performed as described in Methods. The lanes demarked U, G, C and A are dideoxy sequencing reactions. ***c***, Sequence and secondary structure of the HCV IRES domain IIIe and IIId RNA oligonucleotides used for the NMR structural studies. Numbering according to Fig. 1*a*. Nucleotides, that were changed to improve transcription efficiency, are outlined.

groove, and are stacked on the 3'adenosine of the sheared G-A pair (Fig. 2*b*).

Functional importance of HCV IRES domain IIIe

The sequence of the GAUA tetraloop is conserved among all HCV isolates, and among related pestiviridae IRES[16]. Our biochemical studies suggest that this loop is a point of direct contact with the 40S subunit. G295, which is exposed to the major groove, is strongly reactive to kethoxal in the free IRES and is protected from chemical modification upon 40S binding (Fig. 1*b*). The importance of the IIIe tetraloop for IRES function was also supported by translation in cultured human HeLa cells. *In vivo* IRES activity of wild type and mutant HCV IRES were measured using a dual luciferase reporter assay. The second cistron contains the firefly luciferase gene, which is translated under IRES control. The size and integrity of the dicistronic mRNAs were monitored by Northern analysis to examine the possibility that firefly luciferase protein was synthesized from functionally monocistronic firefly luciferase-containing mRNAs, which could have been generated by splicing or by cryptic promoter elements located in the discistronic genes. These Northern analyses revealed that all dicistronic mRNAs remained largely intact (data not shown), arguing that the second cistrons were translated by internal initiation mediated by the HCV IRES.

Using the dual luciferase reporter assay, we studied the effects of mutations of the GAUA tetraloop motif on IRES activity. Mutation of the major groove exposed base U297 to a cytosine residue causes a more than 50% decrease in IRES-mediated translation compared to wild type (Table 1). Converting the GAUA tetraloop into the GNRA tetraloop sequence by mutating U297 to an adenine residue, causes the same decrease in IRES activity. These data are consistent with a previous mutational study of domain IIIe, which showed that virtually any alteration of the loop sequence caused a significant decrease in IRES activity[11]. The presentation of bases by the domain IIIe tetraloop may be required for the IRES-40S subunit interaction.

Structure of HCV IRES domain IIId

The domain IIId RNA forms a helical stem with noncanonical pairings, followed by a hexanucleotide loop region. The overall structure is well defined by the NMR data (heavy atom r.m.s. deviation = 1.61 Å; Fig. 3*a*). The –UUGGGU– hairpin loop is more disordered than the other regions of the RNA; the heavy

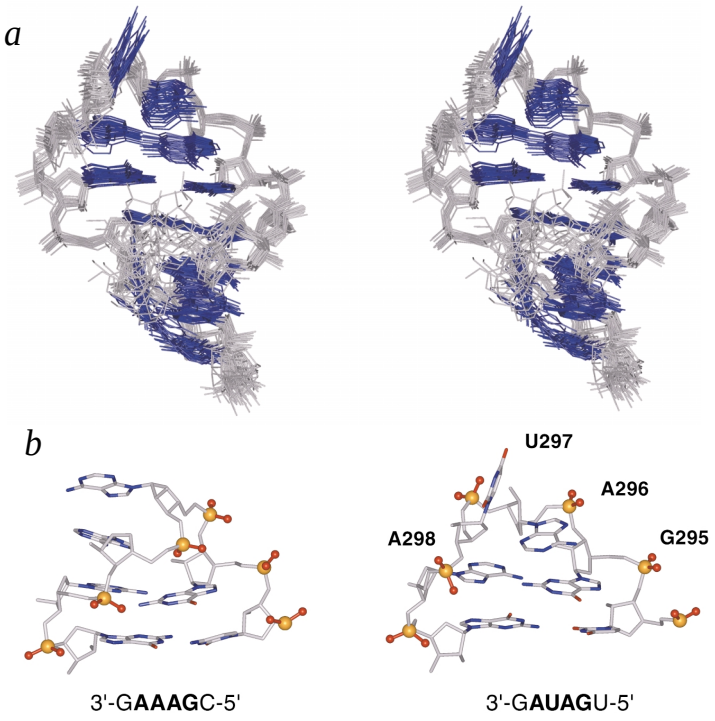

Fig. 2 Structure of HCV domain IIIe stem loop. ***a***, Stereo view from the major groove of the heavy atom superposition of final 20 structures of HCV IRES domain IIIe. Bases are colored in blue and ribose-phosphate backbone in gray. ***b***, Single representative structures of the GNRA[14] and the GAUA tetraloop of HCV IRES domain IIIe. Base nitrogens are in blue and base oxygens in red. Phosphorus atoms and phosphate oxygens are shown explicitly in yellow and red, respectively.

atom r.m.s. deviation for U264–U269 is 1.46 Å (Fig. 3*c*). The central internal loop, which is highly conserved among HCV isolates, adopts the well-characterized loop E fold, and is very well defined by the NMR data (r.m.s. deviation of 0.28 Å; Fig. 3*d*). Four consecutive noncanonical base pairs are formed — a sheared G256-A276 pair, a parallel A257-A275 pair, a reverse Hoogsteen U259-A274 pair and another sheared A260-G273 base pair (Fig. 3*e*). The reverse Hoogsteen hydrogen bonding scheme is supported by the observation of internucleotide $^{2}J_{NN}$ scalar couplings. The arrangement of the base pairs within the loop E motif creates a continous stack of four adenines (A260 and A274–A276) with their Watson-Crick faces exposed to the minor groove (Fig. 3*d*). The internal loop is asymmetric, with the bulged G258 positioned in the major groove, where it forms a base triple with the U259-A274 reverse Hoogsteen pair (Fig. 3*e*). The phosphodiester backbone undergoes a local reversion of direction at A257 and G258, such that a parallel hydrogen bonding arrangement between A257 and A275 can form. The inversion in backbone direction leads to an S turn in the backbone between G256 to A259 (Fig. 3*b*), which is characteristic for loop E motifs. The unusual backbone geometry within the loop E motif results from non A-form values for torsion angles β for G258 and A274 (*gauche*$^{+}$), γ for A274 (*trans*), and ε for A257 (*gauche*$^{+}$) to allow for the triple formation and backbone inversion. The structure also explains unusual ^{1}H, ^{13}C, and ^{31}P chemical shifts observed for several loop E resonances (chemical shifts are available on our web page: http://puglisi.stanford.edu/).

Comparison to other loop E motifs

The loop E motif is common in RNAs, with different sequence families[17]. All loop E motifs contain a sheared G-A pair and the adjacent U-A pair. In prokaryotic 5S ribosomal RNA, a loop E motif is observed with a symmetric internal loop: a G-G pair and a sheared G-A pair[18]. In eukaryotic 28S ribosomal RNA, the sarcin-ricin loop (SRL) contains a loop E motif that contains the A-A pair, bulged G, U-A pair and G-A pair[19,20]; the r.m.s. deviation between the crystal structure of SRL and the HCV IRES domain IIId loop E motif is 1.15 Å. The SRL has a flexible region adjacent to the loop E motif, whereas in domain IIId the loop E is bordered by a sheared G-A pair and Watson-Crick base pairs. Loop E motifs present rich hydrogen bonding potential in both the minor and major groove for both RNA–RNA and RNA–protein interactions.

Functional importance of domain IIId

The sequence of the –UUGGGU– hairpin loop of domain IIId is absolutely conserved among all HCV isolates[16]. The hairpin loop is separated from the loop E motif by a short helical stem consisting of a G-U wobble pair flanked by two G-C Watson-Crick base pairs, of which one closes the hairpin loop. On the 5′ side of the loop, U264 stacks on top of the loop closing G-C base pair, whereas U269 on the 3′ side is bulged into solution and disordered in the ensemble of NMR structures (Fig. 3*c*). This positions the ribose of G268 above the ribose of C270 of the loop-closing G-C base pair, which exposes the base of G268 to the major groove and introduces an inversion in backbone direction similar to the loop E motif with an S turn between G267 to C270 (Fig. 3*b*). G267 stacks below G266 in the minor groove of the loop and U265 is located in the major groove, where it loosely stacks on the 5′ side residues and is more disordered compared to the three guanosine residues. The six base pair spacing between the loop E and the hairpin loop backbone reversion places both S turns on the same side of the hairpin loop structure. This creates a unique backbone feature for the domain IIId motif.

The domain IIId hairpin loop clearly plays an important role in IRES–40S subunit interaction. In the chemical probing

Table 1 Translational efficiencies of HCV IRES elements

Genotype[1]	Activity (%)[2]
Wild type	100
U297C	45 ± 2.1
U297A	47 ± 4.0
G266-268a	48 ± 3.7

[1]All dicistronic vectors contain an additional mutation of the HCV AUG start codon to CUG, which did not affect translational activity[6].
[2]Translational efficiency of mutant IRES RNAs is displayed as LucF/LucR ratio in reference to wild type IRES RNA, whose LucF/LucR ratio was set to 100% activity. Mean values from four independent transfection experiments performed as duplicates are shown with standard errors. The size and integrity of the dicistronic mRNAs were monitored by Northern analysis (data not shown). All mRNAs displayed similar intracellular stabilities, confirming that the second cistrons (LucF) were translated by internal initiation mediated by the IRES element.

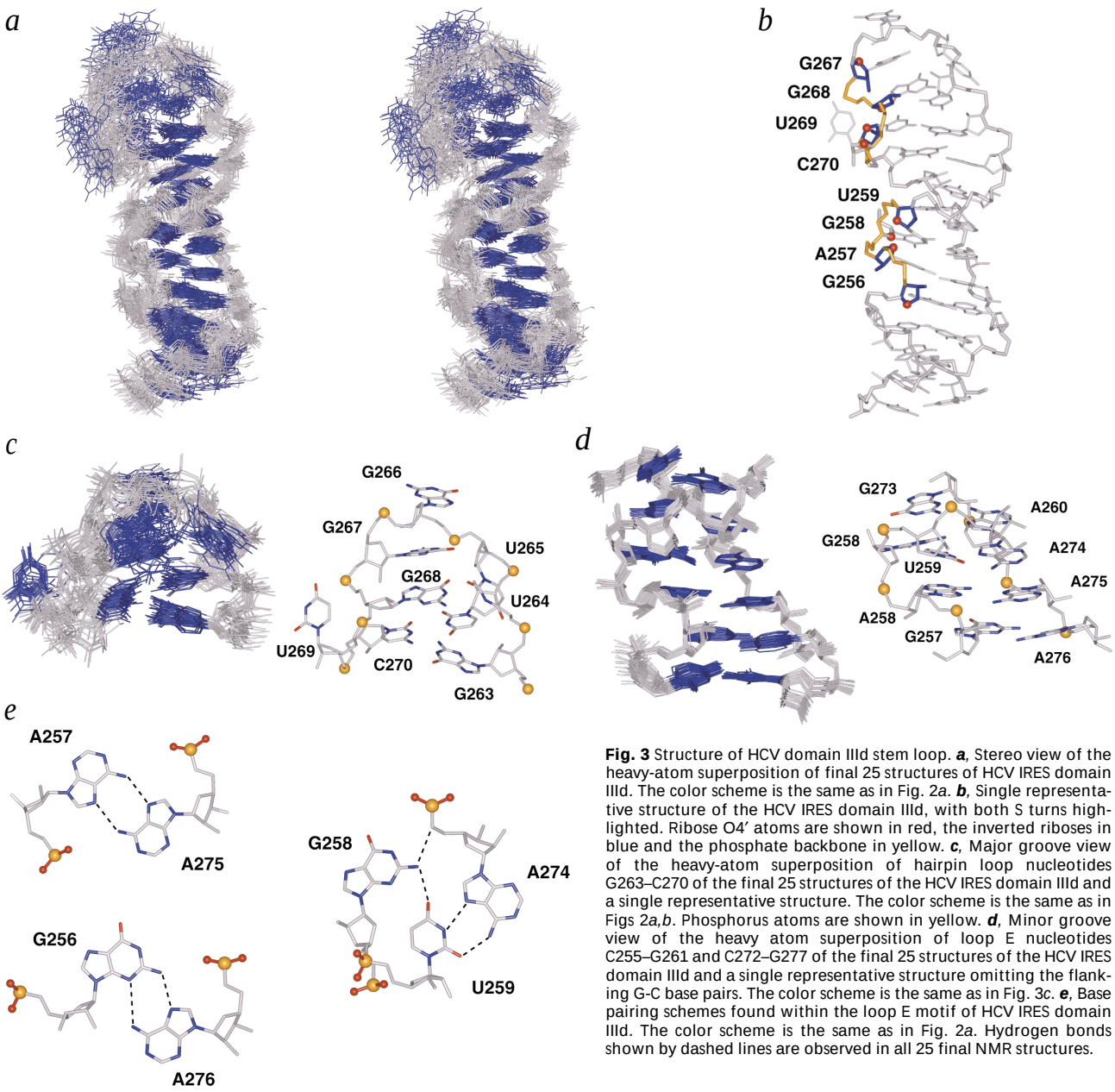

Fig. 3 Structure of HCV domain IIId stem loop. ***a***, Stereo view of the heavy-atom superposition of final 25 structures of HCV IRES domain IIId. The color scheme is the same as in Fig. 2*a*. ***b***, Single representative structure of the HCV IRES domain IIId, with both S turns highlighted. Ribose O4′ atoms are shown in red, the inverted riboses in blue and the phosphate backbone in yellow. ***c***, Major groove view of the heavy-atom superposition of hairpin loop nucleotides G263–C270 of the final 25 structures of the HCV IRES domain IIId and a single representative structure. The color scheme is the same as in Figs 2*a*,*b*. Phosphorus atoms are shown in yellow. ***d***, Minor groove view of the heavy atom superposition of loop E nucleotides C255–G261 and C272–G277 of the final 25 structures of the HCV IRES domain IIId and a single representative structure omitting the flanking G-C base pairs. The color scheme is the same as in Fig. 3*c*. ***e***, Base pairing schemes found within the loop E motif of HCV IRES domain IIId. The color scheme is the same as in Fig. 2*a*. Hydrogen bonds shown by dashed lines are observed in all 25 final NMR structures.

experiments discussed above, the Watson-Crick faces of G266, G267 and G268 were strongly protected from reaction with kethoxal in the IRES–40S subunit complex (Fig. 1*b*). In addition, the N7 positions of G266 and G267 are protected from methylation by dimethyl sulfate (DMS) in the IRES–40S complex, whereas the N7 of G268, which is exposed on the major groove side of the IIId loop, is highly reactive in the complex (data not shown). The three guanosines in the loop are required for full IRES activity in internal initiation. Mutation of the three loop guanosines to cytosines had been previously shown to be deleterious to IRES activity *in vitro*[12]. Based on our structural data, we mutated all three guanosine residues (G266-G268) to adenines preserving purine residues in those positions in order to maintain the fold of domain IIId, which was tested by chemical probing (data not shown). These mutations, which did not alter the local IRES fold like the G266-268C mutations, decreased IRES–mediated translation by 50% (Table 1).

What is the role of the loop E motif in domain IIId?

The ability to form a loop E fold is conserved among HCV isolates. An observed change is G256-A276 to a U-C pair in HCV isolate HCV-2b, which would lead to the SRL loop E motif. Our preliminary data indicate that mutations that disrupt both the loop E motif and folding of domain IIId are deleterious to IRES function (data not shown). The loop E motif, with its narrowed major groove, distorted phosphodiester backbone, and stretch of noncanonical pairings, may be involved in RNA tertiary interactions within the IRES, or intermolecular interactions with the 40S subunit; the interactions with the ribosome may be with protein or RNA components. The adenosine N1 positions of A274–A276 in the minor groove of the loop E

Table 2 Structural statistics for domain IIIe and IIId RNA oligonucleotides

	domain IIIe <SA>[1]	domain IIId <SA>[2]
Total number of experimental restraints		
Distance restraints	271	705
Dihedral restraints	88	200
Final distance and dihedral restraint		
Violation energies (kcal mol^{-1})	15.9 ± 0.8	29.9 ± 0.7
R.m.s. deviation from experimental restraints		
Distance restraints (Å)[3]	0.03 ± 0.001	0.03 ± 0.001
Dihedral restraints (°)[3]	0.95 ± 0. 0.043	0.98 ± 0.06
Deviations from idealized geometry		
Bonds (Å)	0.0004 ± 0.0001	0.004 ±0.0001
Angles (°)	0.84 ± 0.01	0.86 ± 0.01
Impropers (°)	0.22 ± 0.01	0.25 ± 0.01
	<SA> *versus* SA	<SA> *versus* SA
Heavy-atoms r.m.s. deviation (Å)		
All IIIe RNA	0.89	
All IIId RNA		1.61
Heavy-atoms r.m.s. deviation (Å)		
IIIe loop (U294–G299)	0.19	
IIId loop E motif (G256–A260, G273–A276)		0.28
IIId hairpin loop (U264–U269)		1.46

[1]<SA> refers to the final 20 simulated annealing structures, SA to the average structure obtained by taking the average coordinates of the 20 simulated annealing structures best-fitted to one another.
[2]<SA> refers to the final 25 simulated annealing structures, SA to the average structure obtained by taking the average coordinates of the 25 simulated annealing structures best-fitted to one another.
[3]The final structures did not contain distance violations of >0.25 Å or dihedral violations of >5°. Numbers in parentheses refer to number of restraints.

motif are highly accessible to modification by DMS in the IRES–40S subunit complex (Fig. 1*b*). Therefore, protein or RNA interactions with the loop E motif likely occur on the major groove side. Additional experiments are required to determine the precise role of the loop E motif of domain IIId in IRES–40S subunit interaction.

The results presented here demonstrate that two surface-accessible stem loops in the HCV IRES are involved in complex formation with 40S ribosomal subunits. The novel structures of both domain IIId and IIIe are suggestive of their involvement in IRES function, and suggest experiments for a molecular level understanding of HCV IRES function. The work presented here demonstrates the powerful ability of RNA NMR to provide local structural information to drive biochemical studies of a large RNA system.

Methods

Sample preparation. RNA oligonucleotides were prepared by transcription from DNA templates by phage T7 RNA polymerase and purified using polyacrylamide gel electrophoresis[21]. Unlabeled and ^{13}C, ^{15}N-labeled RNAs were prepared. Labeled nucleoside triphosphates were prepared in-house using published methods[22]. RNAs were electroeluted from the gel and subsequently dialyzed against final buffer (10 mM Na phosphate, pH 6.4, 1 mM d_{12}-EDTA, 4% D_2O or 100% D_2O). NMR samples were prepared in a Shigemi NMR tube (sample volume 250 μL) at RNA concentrations of 1.0–2.5 mM.

NMR spectral analyses. NMR data were acquired at either 15 or 25 °C on Varian Inova 500 MHz and 800 MHz NMR spectrometers equipped with triple resonance x,y,z-axis gradient probes. ^{1}H, ^{13}C, ^{15}N, and ^{31}P assignments were obtained using standard homonuclear and heteronuclear methods optimized for RNA structure determination (RnaPack, Varian User Library). In short, constant time HSQC, 3D HCCH-TOCSY, 3D HCCH-COSY, and 2D HCCH-RELAY experiments were used to assign sugar spin systems, while through-backbone assignments were made with HCP and HP-COSY experiments[23]. Base exchangeable protons were assigned by correlation to non-exchangeable base protons using heteroTOCSY methods. Intranucleotide H1′ to base proton correlations were obtained using a 2D MQ–HCN experiment[24]. NOE distance restraints from non–exchangeable protons were obtained from 2D–NOESY experiments (100% D_2O) with mixing times of 50, 150 and 250 ms. Exchangeable proton NOEs were determined using SS-NOESY[25] or WATERGATE-NOESY experiments (4% D_20) with mixing times of 50 and 150ms. A 3D ^{13}C-edited NOESY-HSQC experiment (4% D_2O) with a mixing time of 150ms was used to confirm both nonexchangeable and exchangeable proton NOE assignments. Base pairing schemes for IIId were established using the HNN-COSY experiment[13]. NOEs from exchangeable protons were characterized as strong (0–3.5 Å), medium (0–4.5 Å) or weak (0–6 Å), while NOEs from nonexchangeable protons were characterized as either strong (0–3 Å), medium (0–4 Å), weak (0–5 Å) or very weak (0–6 Å). Dihedral torsion restraints were obtained from DQF-COSY, 3D HMQC-TOCSY, HP-COSY and HCP experiments, as described[26]. Spectra were analyzed with SPARKY[27].

Structure calculation. Structures were calculated using a simulated annealing protocol within the X-PLOR 3.1 package[28]. The protocol for structural calculations included two stages; simulated annealing of starting structures with random angles and restrained molecular dynamics (rMD) refinement. A total of 699 NOE distance restraints, 6 NN hydrogen bond distance restraints and 200 dihedral restraints for IIId and 271 NOE distance restraints and 88 dihedral restraints for IIIe were used. The NOE distance force constants were set to 50 kcal mol^{-1} $Å^{-2}$ and torsion angle force constants were varied from 5 to 50 kcal mol^{-1} rad^{-2} during calculations. No hydrogen bonding restraints other than experimentally measured ones were used in calculations.

A total of 100 starting structures were generated and subjected to a simulated annealing protocol. This consisted of 500 cycles of energy minimization, followed by rMD at 1,000 K with low values for interatomic repulsion, and subsequent rMD with increasing values for interatomic repulsion while cooling to 300 K. A final minimization step with 1,000 cycles was performed, which included a Lennard-Jones potential and no electrostatic terms. The 100 structures were then subjected to a refinement procedure: 500 steps of restrained energy minimization; rMD at 1,000 K while increasing the torsion angle force constant; rMD while cooling to 300 K and finally 1,000 cycles of energy minimization, which included a Lennard-Jones potential, but no electrostatic terms. The final structures (25 IIId or 20 IIIe) were chosen, which had the lowest total and restraint violation energies, whereas non converged structures were at least one standard deviation higher in total and restraint violation energy (Table 2).

Chemical probing. 40S subunits were isolated from HeLa S3 cell pellets (National Cell Culture Center) by the puromycin method of Blobel and Sabatini[29]. HCV IRES RNA (nt 40–375) was generated by T7 RNA polymerase run-off transcription and purified by gel electrophoresis[12]. Chemical modification with kethoxal and DMS was performed essentially as described in Moazed and Noller[30]. Reactions were performed with an excess of 40S subunits in 125 mM KOAc, 10 mM $MgCl_2$, 30 mM HEPES-KOH (pH 7.0) and 0.5 mM spermidine. Sodium borohydride reduction and aniline-induced strand scission of DMS modified IRES was also performed[31].

Primer extension, using a primer complementary to the HCV IRES open reading frame was used to detect sites of RNA base modification[32]. Body labeled products were separated on an 8% 7 M Urea, 1X TBE acrylamide gel and detected by autoradiography.

Construction of dual luciferase reporter constructs and translation assays. Wild type[1] and mutated HCV IRES elements were subcloned into the intercistronic region of a dicistronic luciferase reporter construct, as described previously[33].

DNA plasmids were transfected into HeLa cells using the FuGENE 6 transfection reagent (Boehringer Mannheim). Transfected Cells were harvested 24 h after transfection and luciferase activities were measured using the Dual Luciferase Reporter Assay System (Promega Biotech).

Northern analysis. Total RNA was harvested from transfected HeLa cells 24 h after transfection using the Trizol reagent (Gibco/BRL). Polyadenosine-containing (polyA$^+$) RNA was isolated from the total RNA using the Oligotex mRNA Kit (Qiagen). Approximately 1 μg of polyA$^+$ RNA was separated on a formaldehyde-containing gel and transferred to a nitrocellulose membrane. Radiolabled probe was generated from a PCR product corresponding to nucleotides 648–1,280 of the firefly luciferase gene using the RadPrime Kit (Gibco/BRL) and hybridized to the membrane using Express-hyb solution (Clonetech).

Coordinates. The cooridinates have been deposited in the Protein Data Bank (accession code 1F84 for HCV domain IIId and 1F85 for HCV domain IIIe).

Acknowledgments

The authors thank E. Lau for preparation of labeled nucleotides. Supported by grants from the NIH, the Hutchinson Foundation and Eli Lilly, Inc., and a postdoctoral grant to P. J. L. from the Max Kade Foundation. The Stanford Magnetic Resonance Laboratory is supported by the Stanford University School of Medicine.

Correspondence should be addressed to J.D.P. *email: puglisi@stanford.edu*

Received 10 May, 2000; accepted 3 October, 2000.

1. Tsukiyama-Kohara, K., Iizuka, N., Kohara, M. & Nomoto, A. *J. Virol.* **66**, 1476–1483 (1992).
2. Wang, C., Sarnow, P. & Siddiqui, A. *J. Virol.* **67**, 3338–3344 (1993).
3. Sachs, A.B., Sarnow, P. & Hentze, M.W. *Cell* **89**, 831–838 (1997).
4. Pestova, T.V., Shatsky, I.N., Fletcher, S.P., Jackson, R.J. & Hellen, C.U. *Genes Dev.* **12**, 67–83 (1998).
5. Fukushi, S. *et al. Biochem. Biophys. Res. Com.* **199**, 425–432 (1994).
6. Reynolds, J.E. *et al. EMBO J.* **14**, 6010–6020 (1995).
7. Rijnbrand, R. *et al. FEBS Lett.* **365**, 115–119 (1995).
8. Honda, M. *et al. Virology* **222**, 31–42 (1996).
9. Wang, C., Sarnow, P. & Siddiqui, A. *J. Virol.* **68**, 7301–7307 (1994).
10. Wang, C., Le, S.Y., Ali, N. & Siddiqui, A. *RNA* **1**, 526–537 (1995).
11. Psaridi, L., Georgopoulou, U., Varaklioti, A. & Mavromara, P. *FEBS Lett.* **453**, 49–53 (1999).
12. Kieft, J.S. *et al. J. Mol. Biol.* **292**, 513–529 (1999).
13. Dingley, A.J. & Grzesiek, S. *J. Am. Chem. Soc.* **120**, 8293–8297 (1998).
14. Heus, H.A. & Pardi, A. *Science* **253**, 191–194 (1991).
15. Puglisi, E.V. & Puglisi, J.D. *Nature Struct. Biol.* **5**, 1033–1036 (1998).
16. Smith, D.B. *et al. J. Gen. Virol.* **76**, 1749–1761 (1995).
17. Leontis, N.B. & Westhof, E. *J. Mol. Biol.* **283**, 571–583 (1998).
18. Dallas, A. & Moore, P.B. *Structure* **5**, 1639–53 (1997).
19. Correll, C.C., Freeborn, B., Moore, P.B. & Steitz, T.A. *Cell* **91**, 705–712 (1997).
20. Zhang, P. & Moore, P.B. *Biochemistry* **28**, 4607–46015 (1989).
21. Puglisi, J.D. & Wyatt, J.R. *Methods Enzymol.* **261**, 323–350 (1995).
22. Batey, R.T., Inada, M., Kujawinski, E., Puglisi, J.D. & Williamson, J.R. *Nucleic Acids Res.* **20**, 4515–4523 (1992).
23. Marino, J.P. *et al. J. Am. Chem. Soc.* **116**, 6472–6473 (1994).
24. Marino, J.P., Diener, J.L., Moore, P.B. & Griesinger, C. *J. Am. Chem. Soc.* **119**, 7361–7366 (1997).
25. Smallcombe, S.H. *J. Am. Chem. Soc.* **115**, 4776–4785 (1993).
26. Fourmy, D., Yoshizawa, S. & Puglisi, J.D. *J. Mol. Biol.* **277**, 333–345 (1998).
27. Goddard, T.D. & Kneller, D. G. *SPARKY 3.* (University of California, San Francisco; 2000).
28. Brünger, A.T. *X-PLOR Version 3.1: A system for x–ray crystallography and NMR.* (Yale University Press, New Haven, Connecticut; 1993).
29. Blobel, G. & Sabatini, D. *Proc. Natl. Acad. Sci. U. S. A.* **68**, 390–394 (1971).
30. Moazed, D. & Noller, H.F. *Cell* **47**, 985–994 (1986).
31. Peattie, D.A. *Proc. Natl. Acad. Sci. U. S. A.* **76**, 1760–1764 (1979).
32. Stern, S., Moazed, D. & Noller, H.F. *Methods Enzymol.* **164**, 481–489 (1988).
33. Johannes, G., Carter, M.S., Eisen, M.B., Brown, P.O. & Sarnow, P. *Proc. Natl. Acad. Sci. U. S. A.* **96**, 13118–13123 (1999).
34. Brown, E.A., Zhang, H., Ping, L.H. & Lemon, S.M. *Nucleic Acids Res.* **20**, 5041–5045 (1992).